Final Report

Study of the Use of Time-Mean Vortices to Generate Lift for MAV Applications

AFOSR/AOARD Reference Number: AOARD-09-4118

AFOSR/AOARD Program Manager: John Seo

Period of Performance: 9/1/2009 – 4/30/2011

Submission Date: 5/31/2011

PI: Andrew Wo, National Taiwan University

Report Documentation Page

Form Approved
OMB No. 0704-0188

1. REPORT DATE	2. REPORT TYPE	3. DATES COVERED
07 JUN 2011	**FInal**	**01-09-2009 to 30-04-2011**

4. TITLE AND SUBTITLE
Study of the Use of Time-Mean Vortices to Generate Lift for MAV Applications

5a. CONTRACT NUMBER
FA23860914118

5b. GRANT NUMBER

5c. PROGRAM ELEMENT NUMBER

6. AUTHOR(S)
Andrew Wo

5d. PROJECT NUMBER

5e. TASK NUMBER

5f. WORK UNIT NUMBER

7. PERFORMING ORGANIZATION NAME(S) AND ADDRESS(ES)
National Taiwan University,1 Roosevelt Road, Section 4,Taipei 106,Taiwan,TW,106

8. PERFORMING ORGANIZATION REPORT NUMBER
N/A

9. SPONSORING/MONITORING AGENCY NAME(S) AND ADDRESS(ES)
AOARD, UNIT 45002, APO, AP, 96337-5002

10. SPONSOR/MONITOR'S ACRONYM(S)
AOARD

11. SPONSOR/MONITOR'S REPORT NUMBER(S)
AOARD-094118

12. DISTRIBUTION/AVAILABILITY STATEMENT
Approved for public release; distribution unlimited

13. SUPPLEMENTARY NOTES

14. ABSTRACT
This work presents a novel mechanism to generate lift towards application in micro air vehicles (MAV). Characteristics of time-mean microvortices under a range of conditions were studied via in-plane oscillation of a flat plate with and without suitable micro-structure on the plate?s top surface. Methodologically, experimental approach is first commenced followed by computation to study a wide range of parameter space. The microdevice leverages on Lorentz force to drive the suspended MEMS-based microplate to in-plane resonance. Computational effort centers around optimization of a range of parameters (geometry, frequency, amplitude of oscillation, etc.) to generate time mean lift. Results suggest the mechanism of time-mean vortex generation under periodic in-plane oscillation of a flat plate is predominantly due to nonlinear effect of acoustic streaming near the finite edges. Multiple vortices configuration was also commenced through spatial geometric variation on the plate. Relationship between vortices, pressure distribution and resultant lift are characterized through a range of parameter space. Net lift is found for cases where frequency is high and under large oscillation amplitude. Results should be applicable to realization of lift on MAV since a relatively simple mechanism of in-plane oscillation of a tuned structure is considered quite feasible. This mode of oscillation should be simple to implement in actual practice, and does not require asymmetric flapping of flexible wing.

15. SUBJECT TERMS
Micro Air Vehicles (MAVs), Fluid Dynamics, Flapping Wing

16. SECURITY CLASSIFICATION OF:			17. LIMITATION OF ABSTRACT	18. NUMBER OF PAGES	19a. NAME OF RESPONSIBLE PERSON
a. REPORT **unclassified**	b. ABSTRACT **unclassified**	c. THIS PAGE **unclassified**	**Same as Report (SAR)**	**23**	

Standard Form 298 (Rev. 8-98)
Prescribed by ANSI Std Z39-18

Objectives:

The goal of this proposal is to study generation of lift via in-plane oscillation of a thin-plate/membrane. The approach will involved (1) design of the platform via appropriate actuation method; (2) characterization of the oscillation; (3) computational effort to supplement the experimental approach to illuminate the physics of the problem involved; (4) attempts to generate lift for the thin-plate/membrane. This work serves as a proof-of-concept for lift generation via time-mean vortices, with particular emphasis on application towards MAV.

Status of effort:

It was realized early on in the project that achievement of potential lift will be likely through mechanism of microvortices. Consequently, it is essential to further elucidate mechanism involved prior to demonstration of potential lift. Much effort was exerted to design a suitable experiment to study the issue involved. Towards this end, a suspended microplate was fabricated via MEMS technology and driven to in-plane resonance via Lorentz force, resulting in desired flow features of time-mean microvortices. However, attempt to measure lift directly was not realized due to enormous difficulties encountered. Computational effort was interrogated to determine optimal range of parameters (geometry, frequency, amplitude of oscillation, etc.) to generate time mean lift. Results suggest the mechanism of time-mean vortex generation under periodic in-plane oscillation of a flat plate is predominantly due to nonlinear effect of acoustic streaming near the finite edges. Multiple vortices through spatial geometric variation on the plate's top surface showed viable pressure signature. Net lift was found for cases where frequency is high and under large oscillation amplitude.

Abstract:

This work presents a novel mechanism to generate lift towards application in micro air vehicles (MAV). Characteristics of time-mean microvortices under a range of conditions were studied via in-plane oscillation of a flat plate with and without suitable micro-structure on the plate's top surface. Methodologically, experimental approach is first commenced followed by computation to study a wide range of parameter space. The microdevice leverages on Lorentz force to drive the suspended MEMS-based microplate to in-plane resonance. Computational effort centers around optimization of a range of parameters (geometry, frequency, amplitude of oscillation, etc.) to generate time mean lift. Results suggest the mechanism of time-mean vortex generation under periodic in-plane oscillation of a flat plate is predominantly due to nonlinear effect of acoustic streaming near the finite edges. Multiple vortices configuration was also commenced through spatial geometric variation on the plate. Relationship between vortices, pressure distribution and resultant lift are characterized through a range of parameter space. Net lift is found for cases where frequency is high and under large oscillation amplitude. Results should be applicable to realization of lift on MAV since a relatively simple mechanism of in-plane oscillation of a tuned structure is considered quite feasible. This mode of oscillation should be simple to implement in actual practice, and does not require asymmetric flapping of flexible wing.

Personnel Supported:
Dr. Cheng-Ming Lin and Prof. Andrew Wo

Publications:
Cheng-Ming Lin, Chan-Chia Tseng, Ting-Yuan Tu, Chen-Lin Chen, and Andrew M. Wo, "Size Selectivity and Trapping Efficiency of Single-cell with a Hydrodynamic Well in a Microfluidic Device" The 14th International Conference on Miniaturized Systems for Chemistry and Life Sciences, 2010 (MicroTAS 2010), pp. 1613-1615, 2010.

Interactions:
(a) Cheng-Ming Lin, Chan-Chia Tseng, Ting-Yuan Tu, Chen-Lin Chen, and Andrew M. Wo, "Size Selectivity and Trapping Efficiency of Single-cell with a Hydrodynamic Well in a Microfluidic Device" The 14th International Conference on Miniaturized Systems for Chemistry and Life Sciences, 2010 (MicroTAS 2010), pp. 1613-1615, 2010.
(b) Not applicable.

Inventions:
(a) None
(b) See the completed DD Form 882 attached.

Honors/Awards:
None

Archival Documentation:

1. Introduction

Utilization of vortices to enhanced aerodynamic performance has been substantially studied for many years. The subject has been reviewed by *Annual Review of Fluid Mechanics* covering transition beneath vortical disturbances [1], airplane trailing vortices [2], vorticity dynamics of the oceanic general-circulation [3], and many more.

It is well known that efficient generation of lift on a MAV is a major technological challenge [4-6]. One of the key feature of lift generation in MAV is the vortex system involving both the bound vortex and shed vortices in an unsteady manner. For example, the ratio of instantaneous to steady circulation for a 2D bound/shed vortex system ranges from 0 to close to 1 in approximately five chord lengths [7]. This is indicative that circulation changes in a sufficient rapid manner that the bound/shed vortex system – not an individual vortex – must be considered in an unsteady manner. This is the case not just in a 2D vortex system but in a much more complicated 3D system as well [8]. Consideration of the lift-drag polar provides additional evidence that this vortex system is of prime importance [7]. The scenario that provides the maximum lift-drag ratio is due to that of flapping wing configuration, where non-flapping wing cases result in substantially less performance. Thus overwhelming evidences suggest that vortex-generated lift is of considerable advantage for lift generation for MAV applications. However, flapping wing involved much inherent mechanical complexity. Thus an alternative approach for lift generation in MAV is under studied.

2. Experimental Aspects

2.1 Design of the microdevice

Lorentz force is utilized to drive a microplate to resonance at approximately 140 kHz with one distinct advantage of reducing the complexity of device actuation, instead of embedding the excitation source within the chip, see Fig. 1. Once in resonance, the microplate generates two microvortices near its edges via secondary flow phenomenon of acoustic streaming [9-10].

The main structure of the vortices generator consists of a double-clammed, suspended bridge, combined with a square plate in the middle, as the primary structure, as shown in the 3D sketch of Fig. 1a. When an alternating current (AC) passed through the gold layer on the surface of the suspended bridge in the presence of an external magnetic field B (Nd-Fe-B magnet, < 1 Tesla) perpendicular to the bridge surface, the main structure was forced to oscillate in the third (in-plane) direction. The geometry of the bridge is 1.2μm thick, 20 μm wide, and 750 μm long, with the square microplate (100 μm by 100 μm) in the middle. Figure 1b shows an edge-on view of the micro structure.

2.2 Quality factor of the microdevice

This vortices-generator is a resonant-based actuator operating under liquid with the natural frequency around 140 kHz. This is implied from the rotational velocity of the vortices which maximizes at this frequency, and decays substantially at off-peak frequencies. The maximum displacement of the oscillatory plate is less than 1μm. From this spectral information, the quality factor (Q) is calculated to be about 10, which is indicative of a reasonable resonating device.

2.3 Device fabrication

The suspended structure was fabricated in three steps: thin film deposition, lithography and etching. Each of which will be described in some detail below (see Fig. 2).

2.3.1 Thin film deposition

With silicon as substrate, the suspended microplate was fabricated from silicon nitride (~1 μm), deposited by low pressure chemical vapor deposition system (LPCVD) around 800^{o}C. After completing the thin film deposition, the wafer was placed in E-beam evaporator at low pressure for sputtering the metallic layer onto the wafer surface as electrode. The order of metal to deposit is first chromium (~100 Å thick) then gold (~1500 Å thick) to leverage the chromium layer as adhesion between silicon nitride and gold.

2.3.2 Lithography

In order to define the suspended structure, two masks are needed in the photolithographic process. Thin positive photoresist (Shipley 1813) is used to coat ~1.3 μm thickness on the metallic layer by using a spin coater. The spin procedure of the PR layer is to increase to 800RPM at acceleration of 200 RPM/s and hold for 10 seconds. The second step is to further increase to 4000RPM at acceleration 400 RPM/s and hold for 30 seconds. Then, the wafer was heated by a hot plate at 90°C for 100 seconds. Afterwards, the device was exposed through the first mask by utilizing the UV light (wavelength 365nm) which power is around 15mJ/cm^2 for 5.5 seconds to define the primary microelectrode structure. Developer (MF-319) removed the exposure area when the device was immersed for 1 minute, then stop-develop using DI water to

rinse the surface and N_2 gas dry. The chip was baked at 100^{o}C for 5 minutes to reduce residual solvent.

The purpose of the second mask is to define the cavity underneath the structure, and the total length (750μm) of the beam and the overall features. By repeating the procedure of coating photoresist (S1813), the second mask targets on the key that represents the second pattern has matched with the first pattern. Also, the UV light (wavelength 365nm, power 15mJ/cm^2) was used through the mask for 5.5 seconds, and the chip was subsequently developed by developer (MF-319). Finally, the structure was checked by microscope to make sure the photoresist cover the entire electrode.

2.3.3 Etching

The purpose of the etching steps is to suspend the microplate structure. Silicon nitride that is not protected by the photoresist need to be etched using reactive ion etching (RIE). During which, CF_4 gas is chosen and includes four parameters: (1) pressure of 7.8 Pa, (2) flow rate of 50 sccm, (3) power of 70 W, and (4) time of 18 minutes.

Next, the unprotected region in the silicon nitride would be etched by potassium hydroxide (KOH). The chip is immersed into alkaline solution whose prescription is KOH：DI water = 1：4. Moreover, the probe temperature is set at 78°C and stirring rod rotating at 180rad/s for 12hours. Finally, the chip is rinsed by DI water and dried by N_2 gas. Fabrication of the suspended structure is then completed.

3. Experimental Effort

Lorentz force is utilized to drive a microplate to resonance at approximately 140 kHz with one distinct advantage of reducing the complexity of actuation (instead of embedding the excitation source within the chip). The dominant effect of the oscillatory microplate's boundary, other than the classical Stokes-like unsteady boundary layer with penetration depth of ~6μm, is generation of a pair of predominantly 2D, time-mean, counter-rotating microvortices. Figure 3a presents micrograph of the microvortices with diameter of 80-100μm (order of the microplate dimension), as made evident through polystyrene tracer particles (10μm) in circular trajectory. Majority of the particles are initially drawn from far above the plate toward the plate center, then, as they approach the surface, directed toward the two edges, ejected outward, looped upward, and re-circulated back towards the plate center – repeating the trajectory. Small number of particles, however, are ejected far beyond the plates' edges and never to return. This data show the microvortices are robust and controllable.

4. Computational Effort

Computation effort complements the experimental findings and provides further insight. Figure 4 presents the computed *time-mean* streamline in the region above the oscillatory microplate. Distinct, symmetric, circulatory streamline patterns are shown. Streamlines are far above the plate and directing toward the center, entering the tight vortex core, with some leaving the core at the far ends while majority of the flow forms the re-circulating pattern. Streamline pattern further suggests large variation of velocity over the plate; streamlines conglomerate just above the plate indicating high-speed flow and are further apart at the top of the vortex. Overlay the trajectory of tracer particles from Fig. 3a onto the computed streamlines shows the two flow

patterns agree well. The computation is thus believed to be capable of capturing the dominant physics, although further study is needed.

With the definitive pair of vortices captured by the experiment, computational effort was commenced to explore vortical flow features that would produce lift. To this end, a range of parameter space was studied. This includes asymmetric geometry between the upper and lower surfaces, frequency and amplitude of oscillation. Decision to embrace this set of variables was guided by physical intuition and non-dimensional analysis.

The moving-mesh technique was utilized for describing the oscillatory boundary in an unbounded half-space field with air as working fluid (ρ =1.0 Kg/m3, ν =1.8e-5 Pa • s). The range of oscillating frequency of the moving plate studied was 1Hz, 10Hz, 100Hz, and 1000Hz. The thickness of the plate (t) is kept fixed at 1 mm. The amplitude of oscillation ranges from 0.1 m (0.1t), 0.2 mm (0.2t), and 0.5 mm (0.5t). Time-mean velocity field, time-mean pressure, and time-mean total force per unit depth were reported at time interval of T*/N (T*= 1/frequency, N= 50, where the N is the number of time steps per cycle) by solving the incompressible Navier-Stokes equation for 20 cycles of oscillation.

As aforementioned, systemic computational study of a range of parameter space was untaken. First, flat plate under in-plane oscillation was commenced which serves as control for subsequent calculations. Figure 6a presents the mesh and the range of physical parameters studied. The geometric parameters include plate thickness (t)= 1mm (fixed); length of plate= 30mm; frequency= 100Hz; amplitude ratio (δ /t)= 0.1, 0.2, 0.5. Much effort was spent to fine-tune the computation to allow for convergence in this 2D unsteady calculation while maximizing grid density.

Figure 6b shows the computed flow features near the right edge of the flat plate. As aforementioned, edge effect plays a key role in lift generation and, as expected, poses difficulty due to singularity involved, requiring special care in handling the numeric. Much effort in trial and error was exerted. Velocity vector results show clear vortical flow features. Due to symmetry of the top and bottom geometry, distinct, symmetric, circulatory flow patterns are also demonstrated. The flow above the plate is directed toward the pate's edge, entering the tight vortex core and forming the re-circulating pattern. The velocity vector pattern further suggests large variation of velocity over the plate; corresponding streamlines conglomerate just above the plate indicating high-speed flow and are further apart at the top of the vortex. The computation is thus believed to capture the dominant physics.

Figure 6c shows the time-mean pressure on the plate's top and bottom surfaces. Results indicate distinct low pressure regions near plate's edges, corresponding to the presence of the vortices on the two surfaces. This further confirms the argument that non-linear acoustic streamlining in the vicinity of the finite edges is the main culprit for the generation of time-mean vortices under purely periodic motion. Although, as expected, the pressure on the top and bottom surfaces are identical hence no net pressure difference across the flat plate, this result suggests that "finiteness of geometry" can be beneficial towards lift generation. Subsequent choice of potential geometry that might incur lift is motivated by this observation.

With the understanding of the flat plate baseline case, insight on the importance of the finiteness of the edges is gained. Leveraging upon this, subsequent design is focused on encouraging geometric spatial gradient along the plate in order to produce vortices, hence should develop lift. To first test this approach, the two edges is designed with vertical extrusion (tip structure) from the edge pointing upward. This design will break the symmetry between the top and bottom surfaces. Further details are provided below.

Figure 7 presents calculations with two extrusion structure placed on each of the two edges to encourage spatial gradient, while the entire structure undergoes in-plane periodic oscillation (see Fig. 7a). Figures 7b and 7c present the captured vortices near the tip edges. Distinct vortical flow features can be seen, each on each side of the extrusion. Resulting pressure distribution further confirms the two vortices via spikes in the signature, as shown in Fig. 7d.

Figure 8 corresponds to having the extruding structure *on* the plate – not just at the edges (see Fig. 8a). This set of results – see Fig. 8b for vortex structure and Fig. 8c for pressure signature – suggest similar trend as that for the extrusion near the edges. This set of results further encourages the use of extruding structure over the entire plate to further maximize lift over the entire plate surface.

Figure 9 presents 2D flat plate under in-plane periodic oscillation with multiple extruding structures on the plate (see Fig. 9a). Parameter space studied include: plate thickness (t)= 1mm (fixed); length of plate= 34mm; distance between extruded structure (h)= 2t; frequency= 1, 10, 100, 1000Hz; amplitude ratio (δ/t)= 0.1, 0.2, 0.5. Figure 9b shows repeated pressure signature – now seems obvious – corresponding to the vortices induced by the extrusion. Table 1 summarized the calculated force for the nine cases. Results confirmed that lift increases as both the frequency and oscillation amplitude increase. The maximize lift computed reaches ~$3.5*10^{-2}$ N/m (per unit depth).

Figure 10 presents this force against Reynolds number, with oscillation velocity and extrusion height as length scale. Figure 10a shows the trend of force increase as the amplitude increases. Figure 10b suggests this trend is near linear in the log-log scale.

Further integration of the approach of multiple extrusions on resultant lift is done via increasing spacing between structures – see Fig. 11a. Figure 11b presents results for pressure signature, while Table 2 summarizes the lift calculated for this geometry for all cases considered. Figure 12 further processes the data for Fig. 11a in terms of Reynolds numbers, and Figs. 12a & 12b are similar in trend to that of Figs. 10a & 10b.

Comparison of data from Table 1 with Table 2 is noteworthy. The two cases give rise to different vortex formation and, thus, difference in resultant lift values. At low frequency (10Hz.), the lift for the extrusion with larger spacing (Fig. 11a) is greater than that with smaller spacing (Fig. 9a). However, at higher frequencies (100Hz. and 1kHz.) this trend is reversed, although not significantly. Nonetheless, it is well known that vortex interacts strongly with surrounding structure and local flow field. And in this flow scenario, the frequency plays a dominant role in determining the final flow features.

Figure 13 shows the result of normalized pressure difference. The x-axis is a modified (unsteady) Reynolds number to describe the oscillatory microplate, and it can be expressed as

$$Re = \left(\frac{\delta t \omega}{\nu}\right),$$

where δ is the amplitude of microplate, t is the thickness of microplate, ω is the frequency of the microplate, and ν is the kinematic viscosity of water. Results show a distinctive trend that the normalized pressure increases with unsteady Reynolds number as well as normalized amplitude. Physically, this results suggest that the pressure difference (closely related to lift) is strongly related to both parameters, with the dependence increase with amplitude ratio. At low amplitude ratio, this effect is much weaker, however.

5. Conclusions

This work presents study of mechanism of generation of lift via in-plane resonance of a microplate with application towards MAV. Instead of some form of flapping wing or out-of-plane motion, simple in-plane oscillation of a basically flat plate is studied experimentally via a MEMS device and numerically. The key result of this work demonstrated that multiple small extruded structure located on the upper surface of the plate induced vortices that resulted in pressure difference between top and bottom surfaces (hence lift). The induced vortices might be further be optimized in order to maximize lift generation.

6. Acknowledgement

Generous funding from AOARD via Grant AOARD-094118 (FA23860914118) is gratefully acknowledged.

[1] P. Durbin et al, "Transition beneath vortical disturbances," Annu. Rev. Fluid Mech. **39**, 107-128 (2007).
[2] P. R. Spalart, "Airplane trailing vortices," Annu. Rev. Fluid Mech. **30**, 107-138 (1998).
[3] P. B. Rhines, "Vorticity Dynamics of the Oceanic General-Circulation," Annu. Rev. Fluid Mech. **18**, 433-497 (1986).
[4] T. Weisfogh et al, "Biology and Physics of Locust Flight. 1. Basic Principles In Insect Flight - A Critical Review." Philosophical Transactions of the Royal Society of London Series B-Biological Sciences 239(667): 415-458 (1956).
[5] W. Shyy et al., "Flapping and flexible wings for biological and micro air vehicles." Progress in Aerospace Sciences 35(5): 455-505 (1999).
[6] K. V. Rozhdestvensky et al, "Aerohydrodynamics of flapping-wing propulsors." Progress in Aerospace Sciences 39(8): 585-633 (2003).
[7] S. P. Sane, "The aerodynamics of insect flight," Journal of Experimental Biology, 206, 4191-4208 (2003).
[8] S. A. Ansari et al, "Aerodynamic Modelling of Insect-like Flapping Flight for Micro Air Vehicles," Progress in Aerospace Sciences, 42, 129-172 (2006).
[9] L. D. Landau et al, *Fluid Mechanics*, 88, (Pergamon Press, 1959).
[10] H. Schlichting, *Boundary-Layer Theory*, 430, (McGraw Hill, 1979).

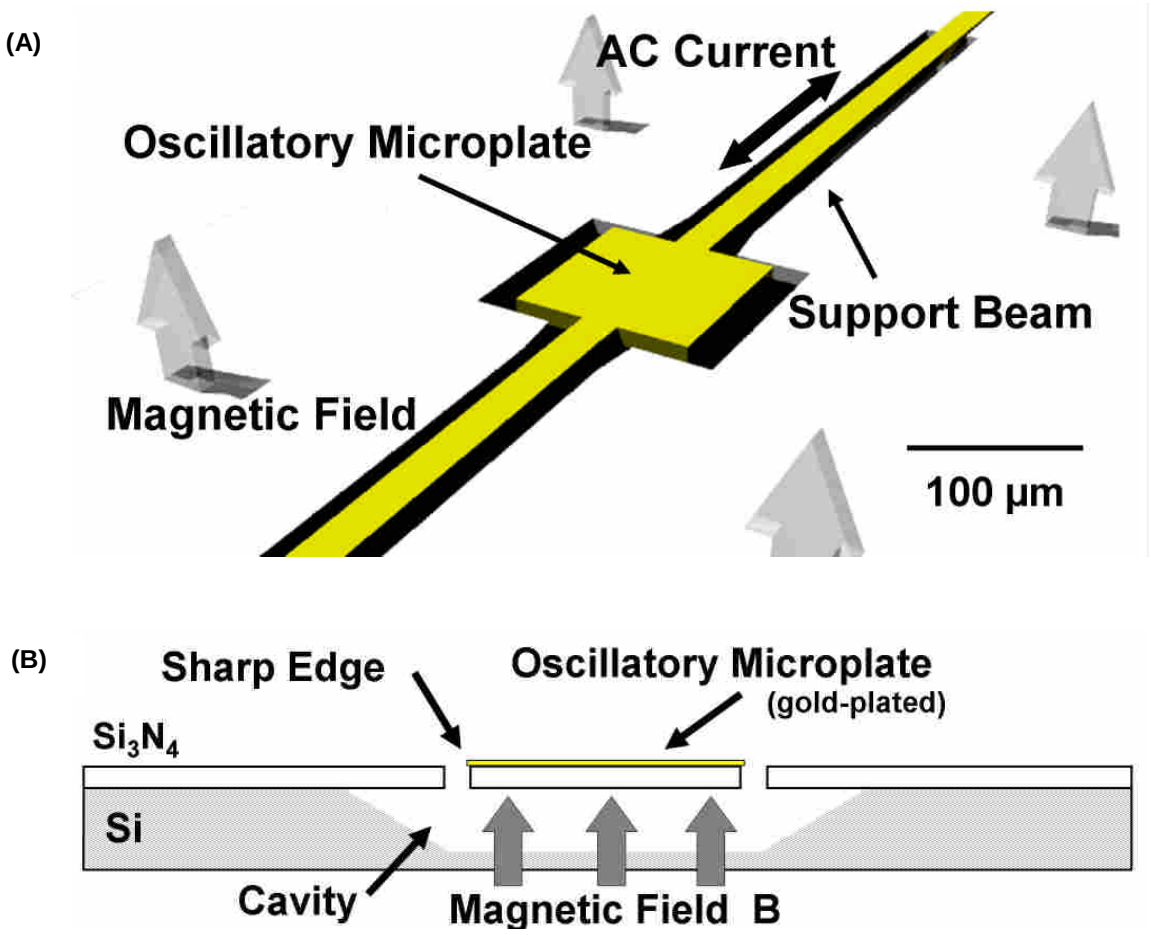

Figure 1. The microdevice. (A) Suspended microplate (100*100*1μm thick) in resonance (140kHz). Plate oscillation is due to Lorentz induced force from AC current flows through the structure above an external magnetic field. (B) Edge-on view showing sharp edges of the microplate, 20μm spacing between microplate and fixed Si_3N_4 structure, cavity underneath, and material details.

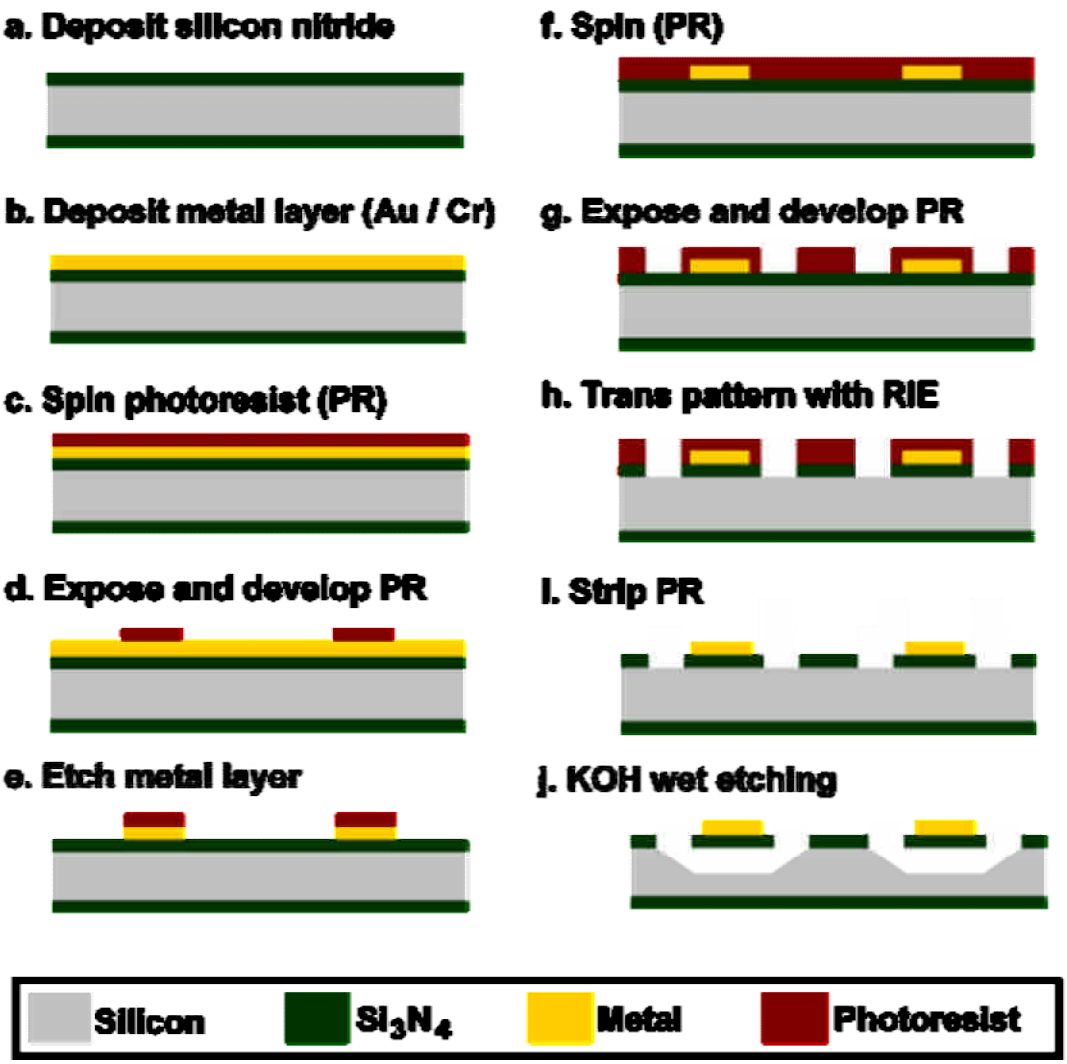

Figure 2. Fabrication processes of the suspended structure. A silicon wafer was used as an experimental substrate. First, the finish on the silicon substrate was silicon nitride (~1μm) (Fig. 2a). Then, a metallic layer (0.15μm thickness of Au/Cr) was sputtered on silicon nitride (Fig. 2b). Moreover, the photoresist (Shipley 1813) layer was patterned for defining the dimension of the electrode (Fig. 2c, d). The element was immerged in the gold and chromium etchant subsequently (Fig. 2e). Next, the positive photoresist on the metal was removed by acetone. By repeating the procedure of coating photoresist (S1813) and development using the MF319 developer (Fig. 2f, g), the cavity underneath the oscillating structure was formed. Therefore, the silicon nitride which was unprotected by the photoresist would be etched using reactive ion etching (RIE) (Fig. 2h). The PR is stripped (Fig. 2i) and etched by utilizing potassium hydroxide (KOH) etchant (Fig. 2j). The suspended structure is finally fabricated.

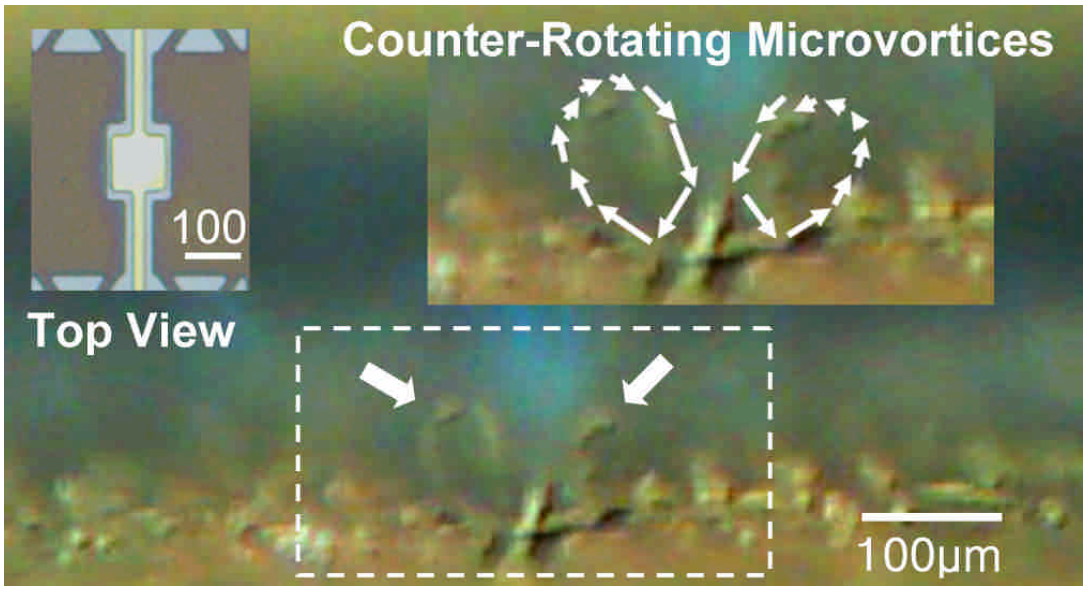

Figure 3. Micrograph revealing counter-rotating microvortices (arrows shown) via tracer particles. The inset (upper left) shows the top view of the device in covered cavity configuration (cover shown in gray regions). Diameter of each vortex (80-100μm) is of order of plate dimension (100μm).

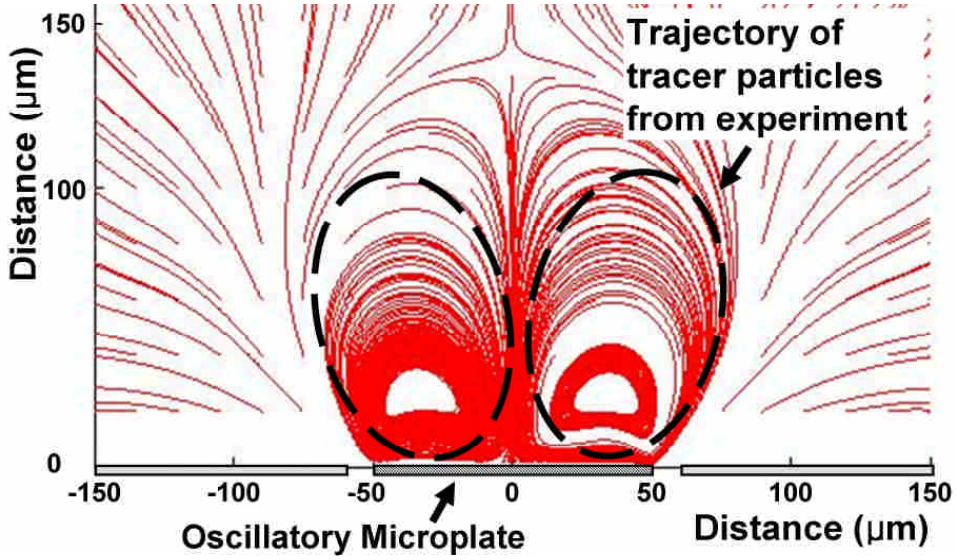

Figure 4. Computational results of the microvortices. Time-mean streamline indicates distinct vortical flow structure. Overlaid are trajectories from tracer particles in the experiment, which show a good match between computed and experimental results of the overall geometry of the microvortices.

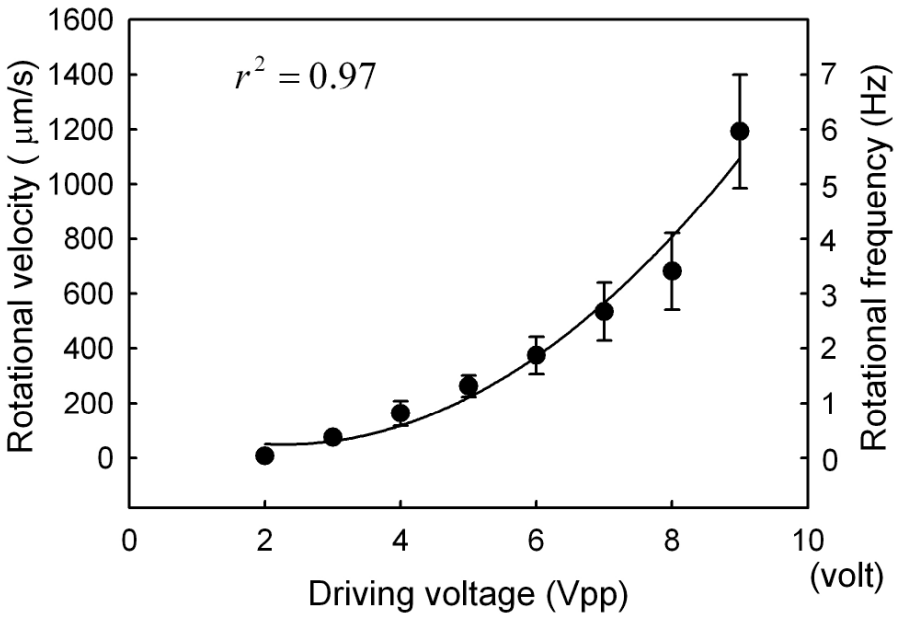

Figure 5. Rotational velocity of a microvortex verses driving voltage (2 to 9Vpp), with corresponding rotational frequency shown on the right ordinate. Results indicated the rotational velocity increases parabolically with voltage. Thus, the microvortex is very controllable, and robust. Statistic analysis performed using Student's t-tests at 95 % confidence level, n = 3, S = 1.0. The regression coefficient is 0.97.

Case 1. Flat plate (baseline)

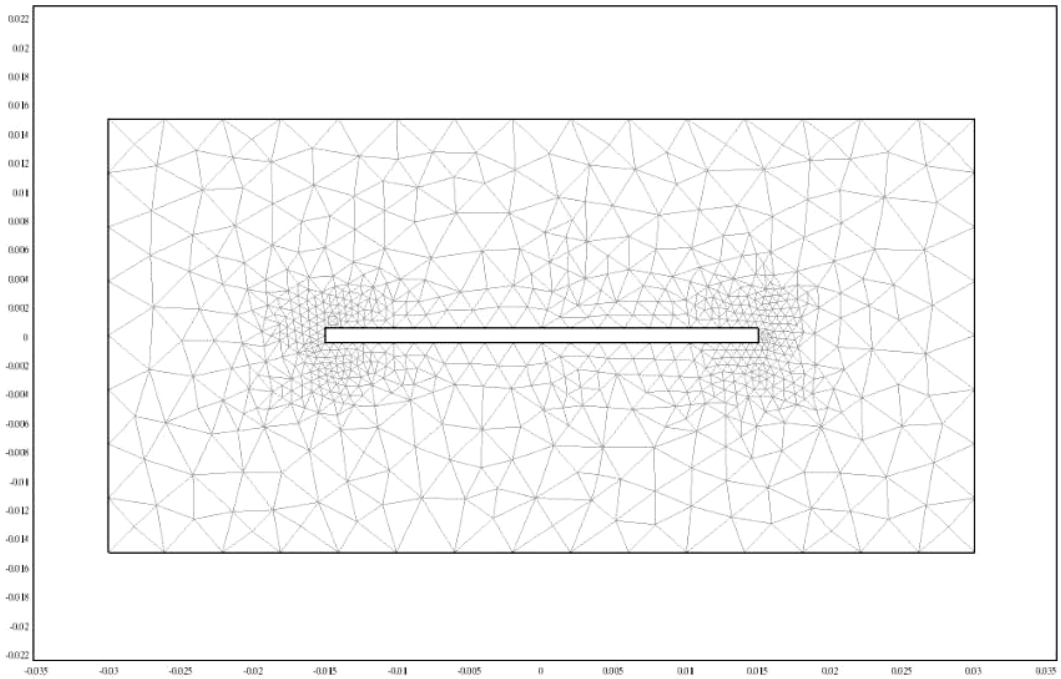

Figure 6a. Mesh of 2D flat plate under in-plane periodic oscillation. Geometric parameters: plate thickness (t)= 1mm (fixed); length of plate= 30mm; frequency= 100Hz; amplitude ratio (δ /t)= 0.1, 0.2, 0.5.

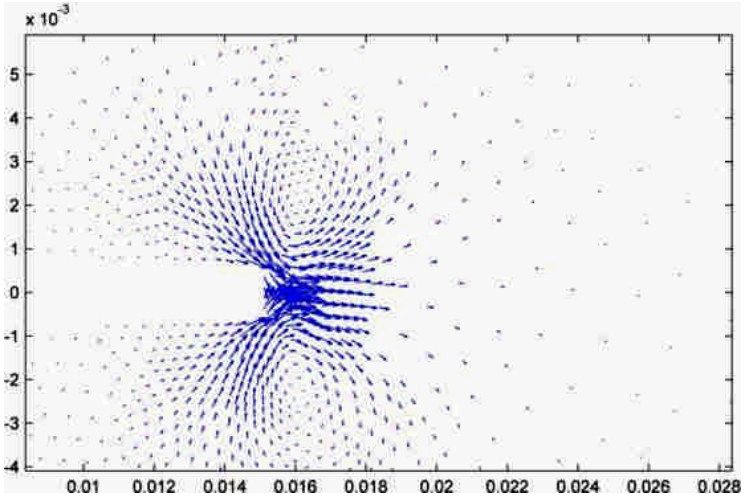

Figure 6b. Time-mean velocity vectors at the plate's right edge showing time-mean microvortices on both the top and bottom regions. This distinct feature corresponds to that observed in the experiment.

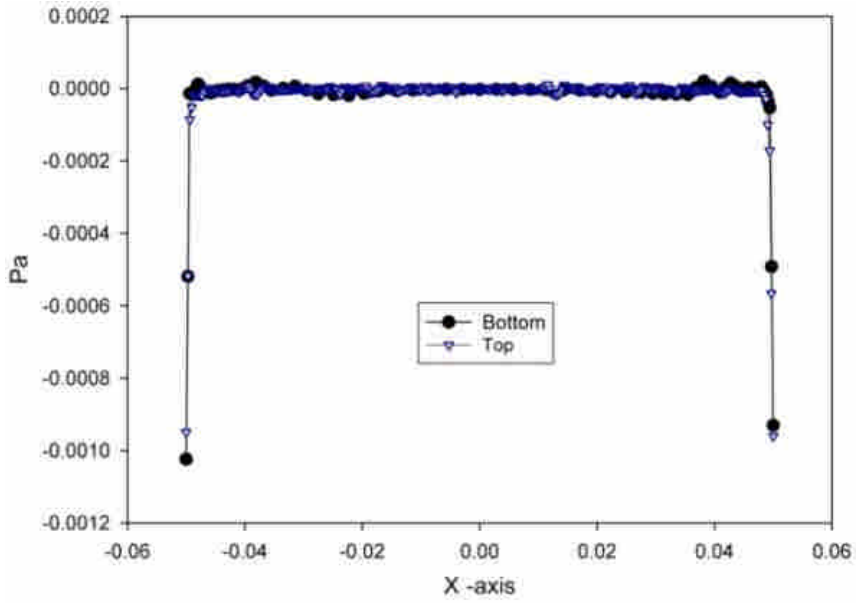

Figure 6c. Time-mean pressure on the top and bottom surfaces. As expected, the pressure trace appears identical; no net pressure difference exists.

Case 2. Tip extrusion structure at the two edges

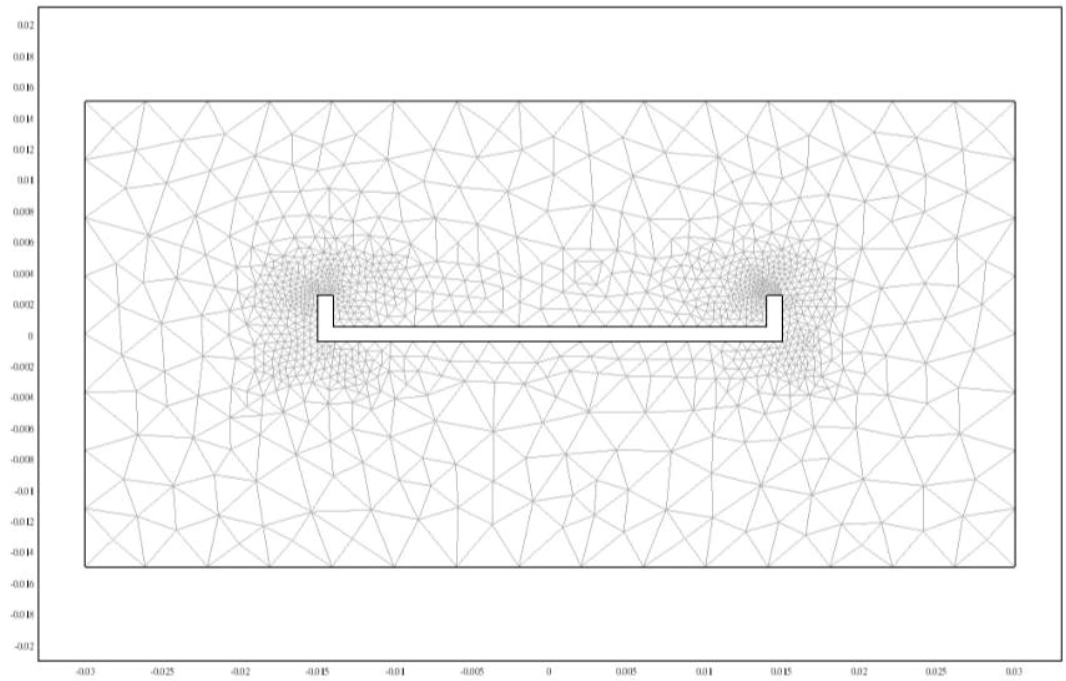

Figure 7a. Extrusion structures are placed on the two edges to encourage spatial gradient, while the entire structure undergoes in-plane periodic oscillation. Geometric parameters: plate thickness (t)= 1mm (fixed); length of plate= 30mm; frequency= 100Hz; amplitude ratio (δ /t)= 0.1.

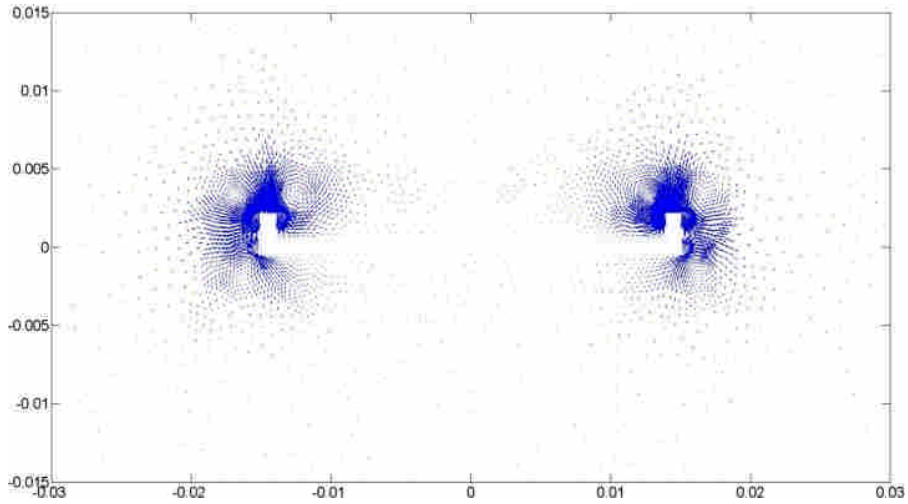

Figure 7b. Time-mean velocity vectors at the plate's edges showing time-mean vortices predominantly on the top surface near the tip structures.

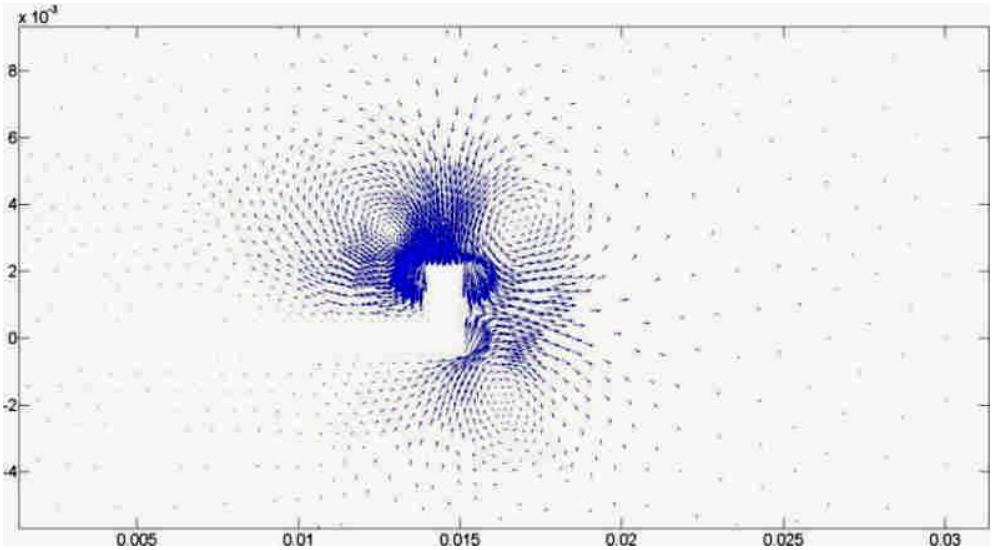

Figure 7c. Close-up of the vortex on the right side of the plate of Fig. 7b.

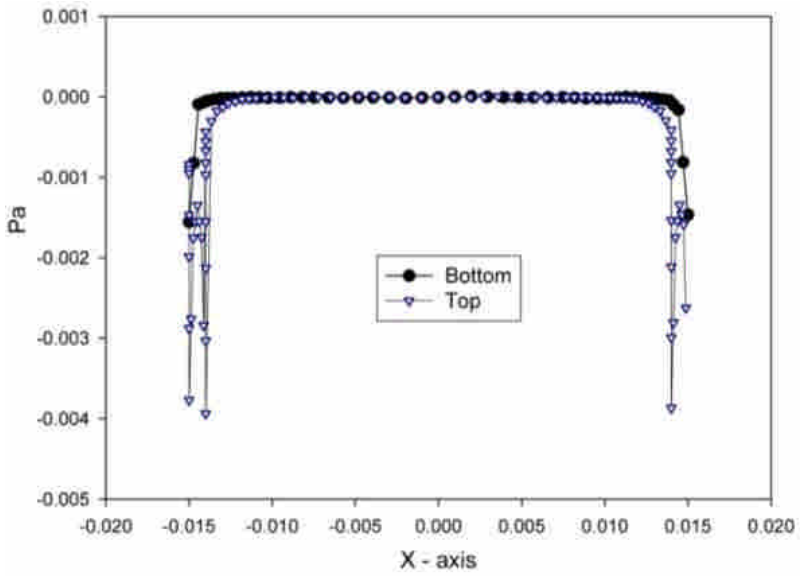

Figure 7d. Time-mean pressure on the top and bottom surfaces. Due to the presence of the tip structure, asymmetry in the pressure signature is shown, unlike that for the purely flat plate case. There exists a relative lower pressure on the extruded structure's edge.

Case 3. A pair of extrusion structure on plate's top surface

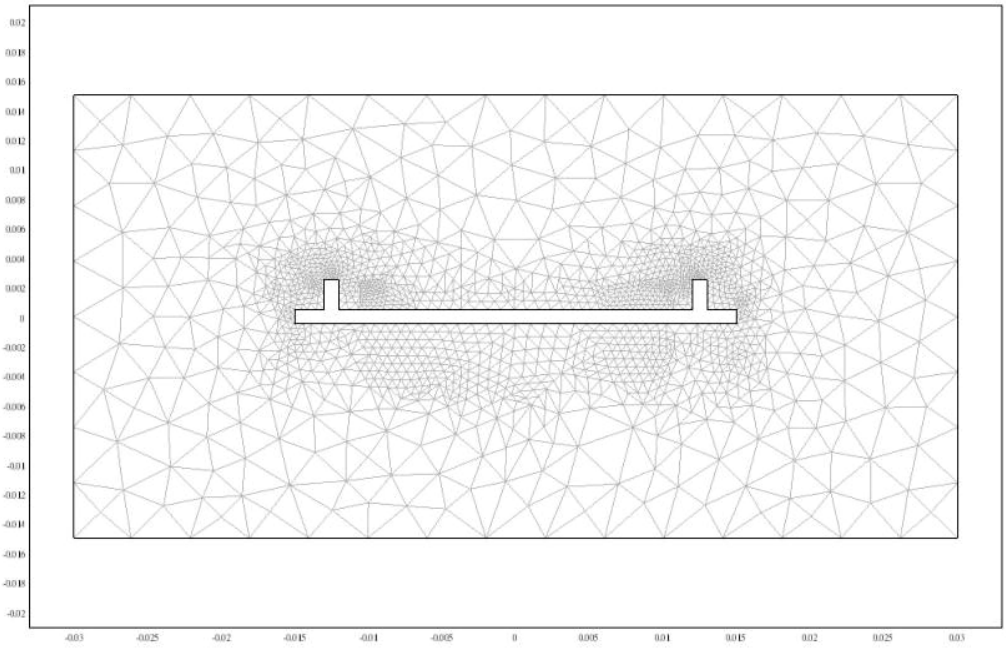

Figure 8a. Mesh of 2D flat plate under in-plane periodic oscillation with a pair of mid-plate extruding structures. Geometric parameters: plate thickness (t)= 1mm (fixed); length of plate= 30mm; frequency= 100Hz.

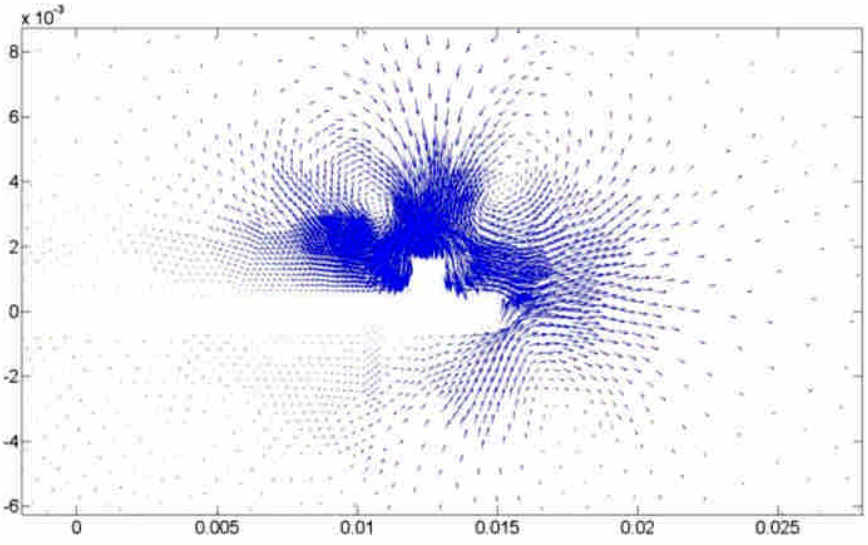

Figure 8b. Time-mean velocity vectors near the plate's extruding structure showing time-mean microvortices on both sides of the extrusion.

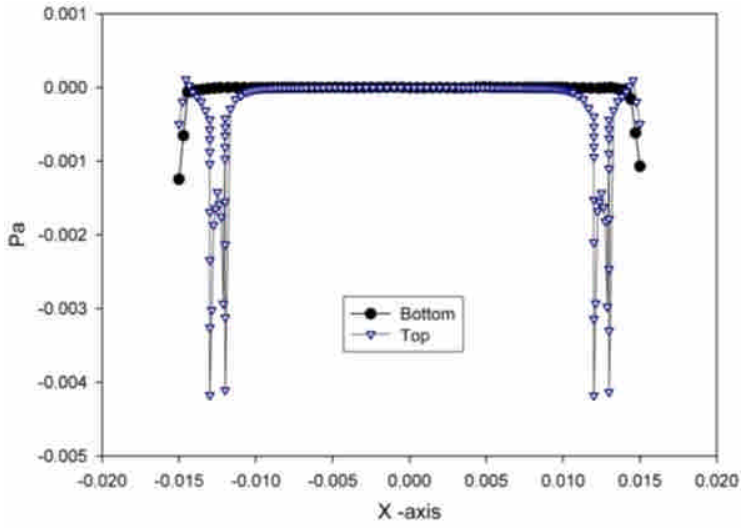

Figure 8c. Time-mean pressure on the top and bottom surfaces. Distinct pressure peaks corresponding to locations of the vortices are clearly seen.

Case 4. Multiple extrusion structure with separation (h)=2*thickness (t)

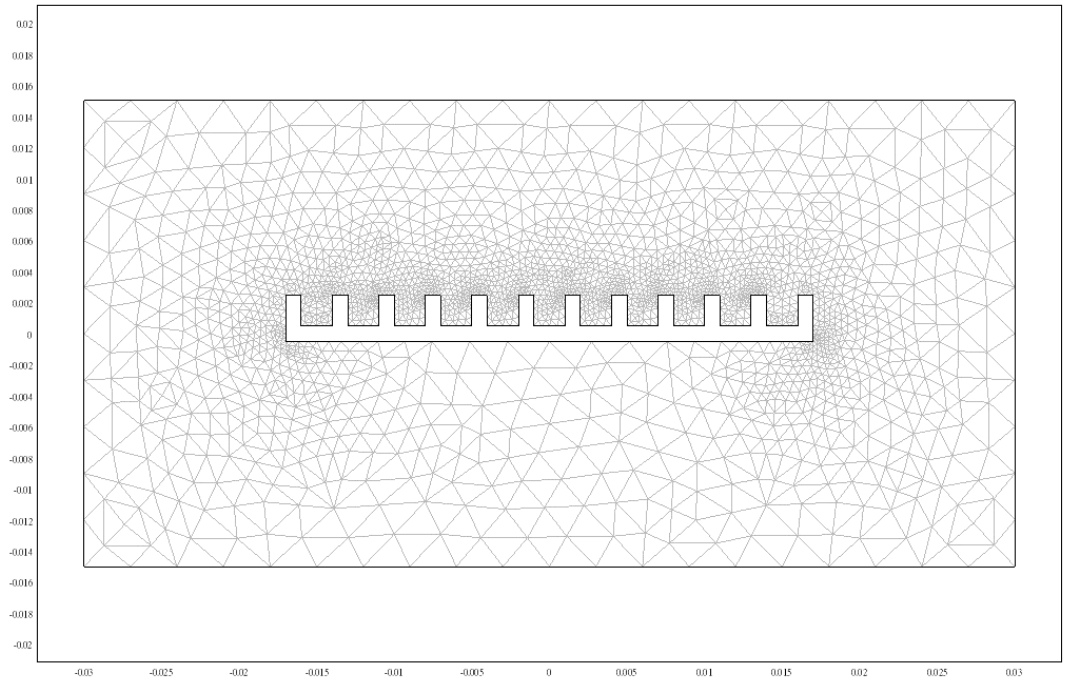

Figure 9a. Mesh of 2D flat plate under in-plane periodic oscillation with multiple mid-plate extruding structures. Geometric parameters: plate thickness (t)= 1mm (fixed); length of plate= 34mm; distance between extruded structure (h)= 2t; frequency= 1, 10, 100, 1000Hz; amplitude ratio (δ /t)= 0.1, 0.2, 0.5.

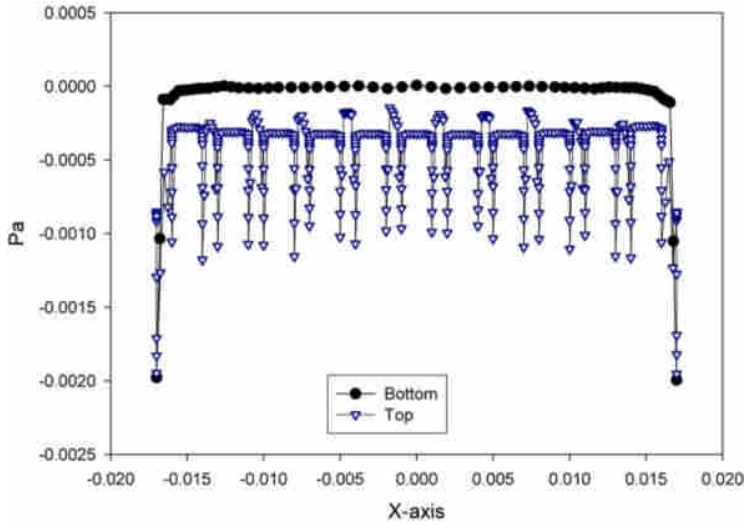

Figure 9b. Typical time-mean pressure distribution on the top and bottom surfaces. Distinct pressure peaks corresponding to locations of a vortex is clearly seen. This pattern of pressure signature is similar over a range of operating conditions, of course, with the exact values of pressure depending on individual cases.

Amplitude ratio (δ /t)	**Force acting on the plate (per unit depth; N/m)**			
	Freq.= 1 Hz.	10 Hz.	100 Hz.	1000 Hz.
0.1	~ 0	-5.54e-10	-2.26e-6	-1.67e-3
0.2	~ 0	-1.9e-9	-1.16e-5	-6.54e-3
0.5	< 10e-10	-1.14e-8	-1.93e-4	-3.49e-2

Table 1. Force acting on the plate corresponding to that of **Fig. 9a**.

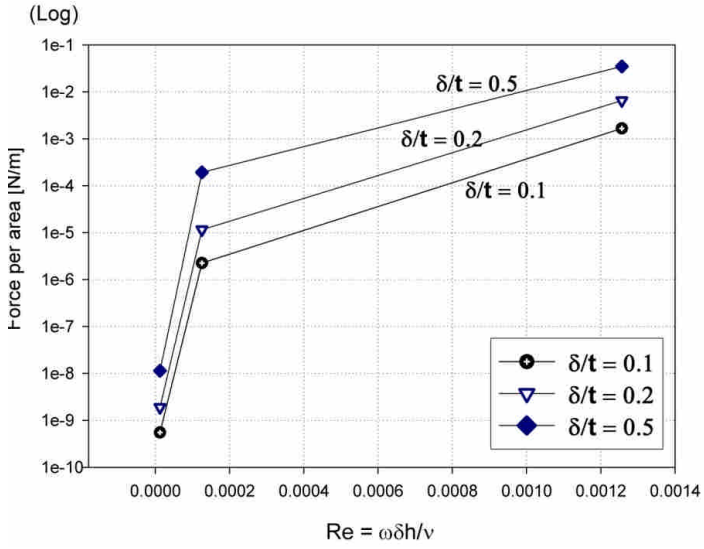

Figure 10a. Dimensionless plot of force (per unit depth) over the range of Reynolds numbers (length scale normalized based on distance between extrusion structures h). Three values of amplitude ratio are shown. Results clearly show strong dependence of dimensionless force with Reynolds number and amplitude ratio.

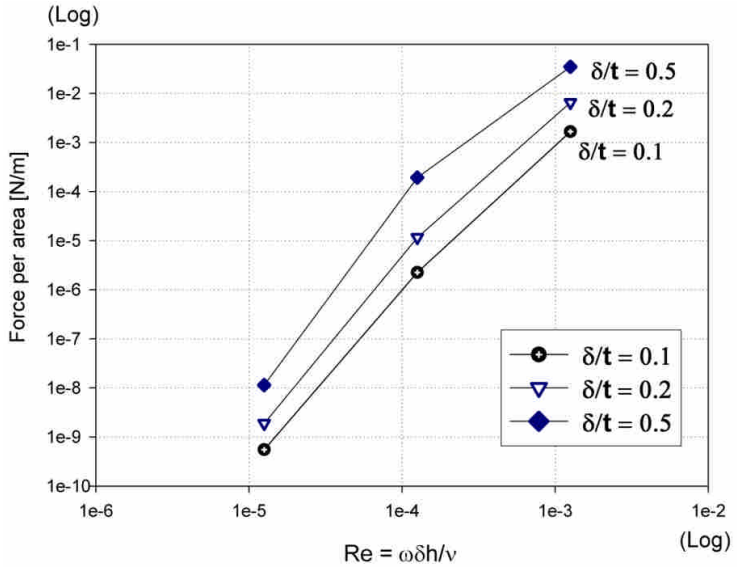

Figure 10b. Same data set as Fig. 10a, except plotted in log-log scale. The near-linearity in this scale is noteworthy.

Case 5. Multiple extrusion structure with separation (h)= 4*thickness

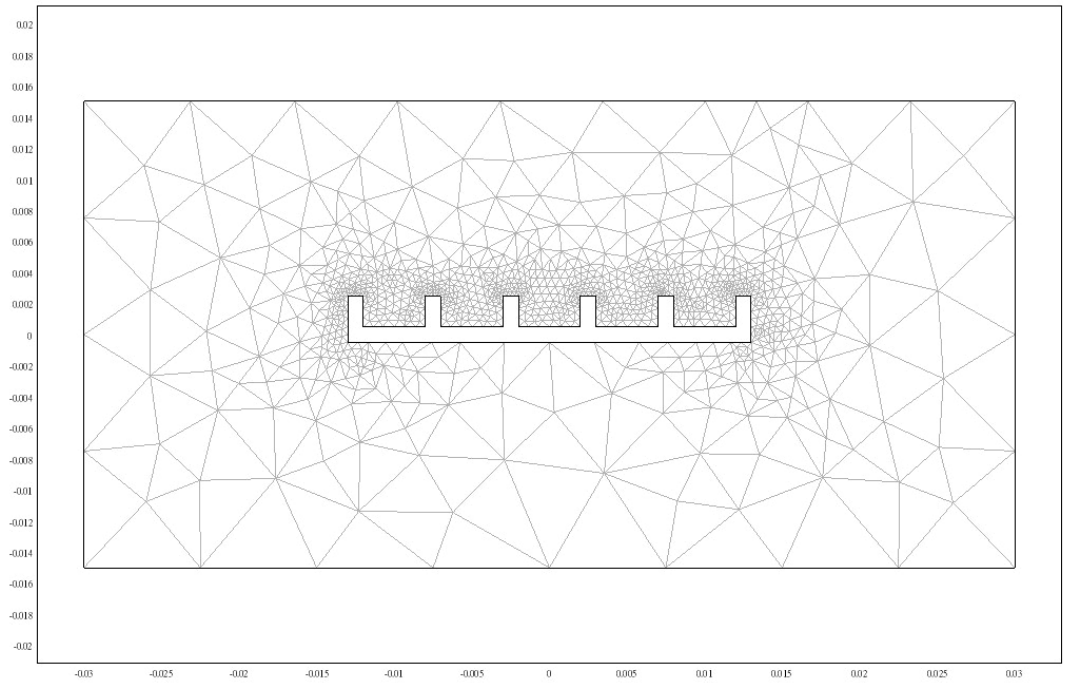

Figure 11a. Mesh of 2D flat plate under in-plane periodic oscillation with multiple mid-plate extruding structures, but each structure further apart than that of Fig. 9a. Geometric parameters: plate thickness (t)= 1mm (fixed); length of plate= 26mm; distance between extruded structure (h)= 4t; frequency= 1, 10, 100, 1000Hz; amplitude ratio (δ /t)= 0.1, 0.2, 0.5.

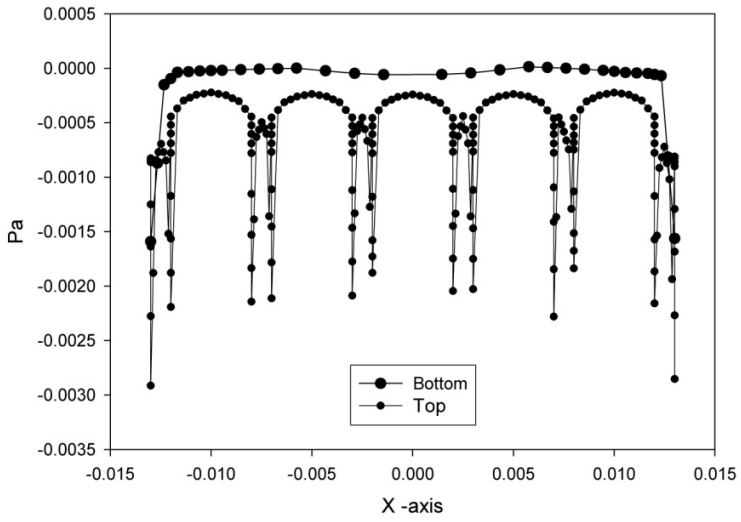

Figure 11b. Typical time-mean pressure distribution on the top and bottom surfaces. Distinct pressure peaks corresponding to locations of a vortex is clearly seen. This pattern of pressure signature is similar over a range of operating conditions, of course, with the exact values of pressure depending on individual cases.

Amplitude ratio (δ /t)	**Force acting on the plate (per unit depth; N/m)**			
	Freq.= 1 Hz.	10 Hz.	100 Hz.	1000 Hz.
0.1	~ 0	-1.29e-9	-1.37e-6	-1.3e-3
0.2	~ 0	-4.44e-9	-7.44e-6	-4.81e-3
0.5	< 10e-9	-4.63e-8	-9.20e-5	-3.53e-2

Table 2. Force acting on the plate corresponding to that of **Fig. 11a**.

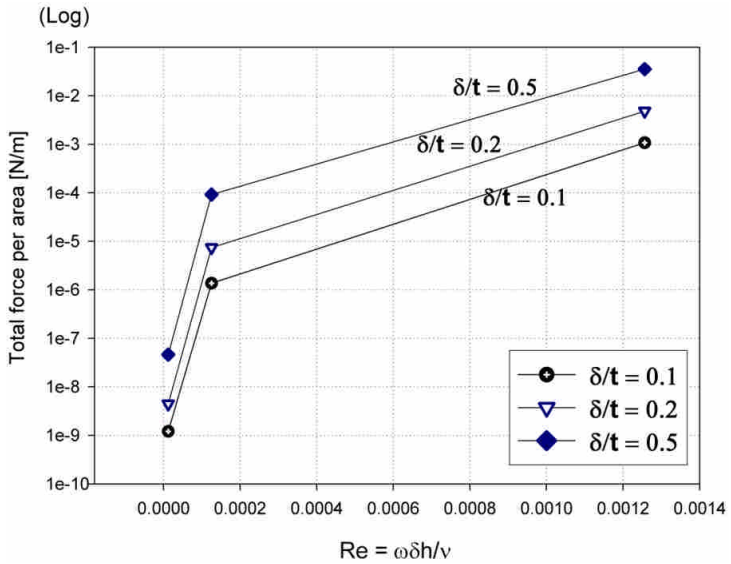

Figure 12a. Dimensionless plot of force (per unit depth) over the range of Reynolds numbers (length scale normalized based on distance between extrusion structures h) corresponding to geometry of Fig. 11a. Three values of amplitude ratio are shown. Results clearly show strong dependence of dimensionless force with Reynolds number and amplitude ratio.

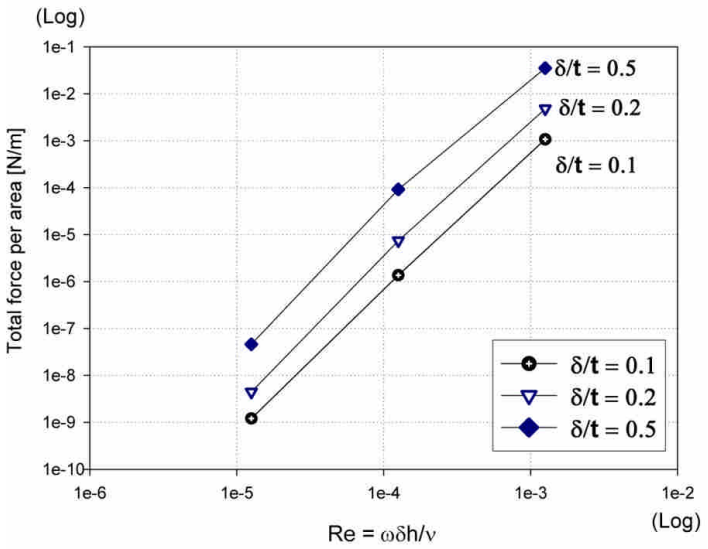

Figure 12b. Same data set as Fig. 12a, except plotted in log-log scale. The near-linearity in this scale is noteworthy.

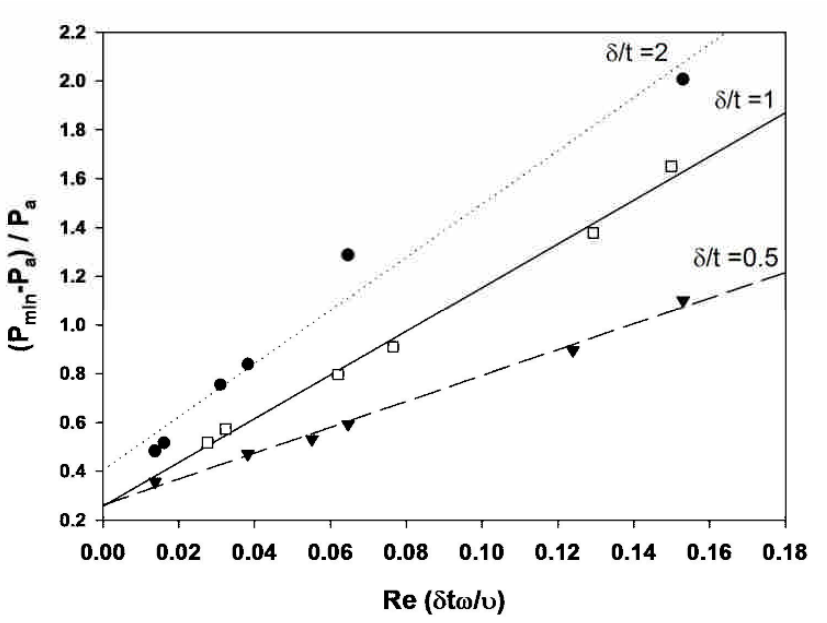

Figure 13. Pressure difference normalized by ambient pressure in the flow field. Results show the normalized pressure difference increases with unsteady Reynolds number of the oscillatory microplate and amplitude ratio (normalized by plate thickness).